LAWRENCE
LIVERMORE
NATIONAL
LABORATORY

UCRL-PROC-216743

Wavelength and pulselength dependence of laser conditioning and bulk damage in doubler-cut KH2PO4

J. J. Adams, J. R. Bruere, M. Bolourchi, C. W. Carr, M. D. Feit, R. P. Hackel, D. E. Hahn, J. A. Jarboe, L. A. Lane, R. L. Luthi, J. N. McElroy, A. M. Rubenchik, J. R. Stanley, W. D. Sell, J. L. Vickers, T. L. Weiland, D. A. Willard

November 1, 2005

Boulder Damage Symposium XXXVII
Boulder, CO, United States
September 19, 2005 through September 21, 2005

Wavelength and pulselength dependence of laser conditioning and bulk damage in doubler-cut KH_2PO_4

J. J. Adams*, J. Bruere, M. Bolourchi, C. W. Carr, M. D. Feit, R. P. Hackel, D. E. Hahn, J. A. Jarboe, L. A. Lane, R. L. Luthi, J. N. McElroy, A. M. Rubenchik, J. R. Stanley, W. D. Sell, J. L. Vickers, T. L. Weiland, D. A. Willard

Lawrence Livermore National Laboratory
7000 East Avenue, L-592
Livermore, CA 94550

ABSTRACT

An experimental technique has been utilized to measure the variation of bulk damage scatter with damaging fluence in plates of KH_2PO_4 (KDP) crystals. Bulk damage in unconditioned and laser-conditioned doubler-cut KDP crystals has been studied using 527 nm (2ω) light at pulselengths of 0.3 - 10 ns. It is found that there is less scatter due to damage at fixed fluence for longer pulselengths. In particular, there is ~4X increase in fluence for equivalent scatter for damage at 2ω, 10 ns as compared to 0.30 ns in unconditioned KDP. The results for the unconditioned and conditioned KDP show that for all the pulselengths the scatter due to the bulk damage is a strong function of the damaging fluence ($\phi^{\sim 5}$). It is determined that the 2ω fluence pulselength-scaling for equivalent bulk damage scatter in unconditioned KDP varies as $\tau^{0.30\pm0.11}$ and in 3ω, 3ns ramp-conditioned KDP varies as $\tau^{0.27\pm0.14}$. The effectiveness of 2ω and 3ω laser conditioning at pulselengths in the range of 0.30-23 ns for damage induced 2ω, 3 ns is analyzed in terms of scatter. For the protocols tested (i.e. peak conditioning irradiance, etc.), the 3ω, 300 ps conditioning to a peak fluence of 3 J/cm^2 had the best performance under 2ω, 3 ns testing. The general trend in the performance of the conditioning protocols was shorter wavelength and shorter pulselength appear to produce better conditioning for testing at 2ω, 3 ns.

Keywords: KDP, DKDP, laser conditioning, bulk damage, pulselength, pulselength-scaling, damage density

1. INTRODUCTION

1.1 General

The current choice for frequency conversion of large aperture kilo-joule class laser systems is KH_2PO_4 (KDP) and KD_2PO_4 (DKDP) [1-2]. Under frequency conversion conditions, crystals of KDP or DKDP can suffer from bulk and surface damage that would adversely affect the quality of the downstream beam. This in turn limits the maximum energy that can be extracted from the laser system. Crystals of KDP and DKDP need to operate with low damage and at both 2ω and 3ω. The as-grown damage performance of these crystals limits the laser beam energy that can be delivered. However, treatment of the crystals with laser-conditioning can improve the bulk damage performance of the crystals above the as-grown limit [3-5]. Laser conditioning is the increase in damage resistance that can occur through exposure to sub-damaging fluences. Specifically for this work, laser conditioning means "ramp" conditioning where the conditioning fluence is ramped in steps to just below the surface damage limit of the crystal or to the output limit of the laser used for the conditioning [5]. Figure 1 a.) is a scatter map image of a virgin or an unconditioned region of a KDP crystal that had been exposed to a single shot at 14 J/cm^2 2ω, 3 ns. Figure 1 b.) is a scatter map image of a region that had first been ramped at 3ω, 3 ns to 8 J/cm^2 in 1 J/cm^2 steps and then exposed to a single shot at 14 J/cm^2 2ω, 3 ns. A scatter map is a dark field image of the damage viewed at perpendicular to its illumination. The bright signals in the photos are scatter from individual bulk damage sites under edge illumination with white light. The ramped (conditioned)

* Correspondence: 925 422-4663, adams29@llnl.gov

region shows very little bulk damage as compared to the unconditioned region thus illustrating the effect of the "laser-conditioning". Historically, bulk damage and laser conditioning effectiveness have both been observed to depend on wavelength and pulselength [5,6]. This paper reports on a systematic and quantitative study of the wavelength and pulselength dependence of bulk damage and laser conditioning in KDP.

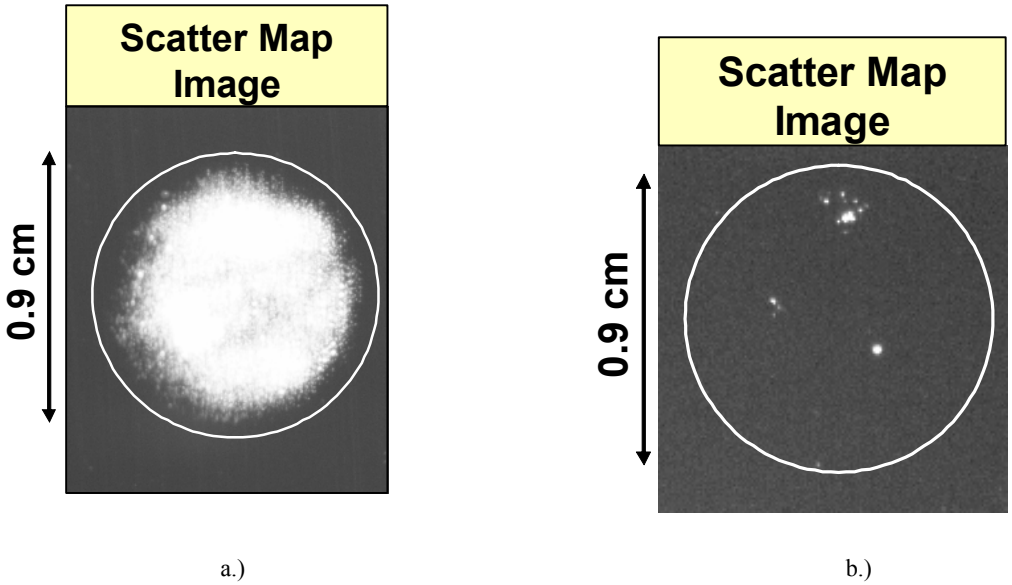

a.) b.)

Figure 1: Scatter map using side illumination with white light of a.) Unconditioned KDP crystal exposed to a single test shot at 14 J/cm^2 2ω, 3 ns. b.) Laser-conditioned KDP crystal with a fluence "ramp" of 2, 3, 4, 5, 6, 7, 8 J/cm^2 3ω, 3 ns and then exposed to a single 14 J/cm^2 2ω, 3 ns test shot.

2. EXPERIMENTS

2.1 Conditioning and Test Facilities

Many of the conditioning and bulk damage experiments were conducted in Lawrence Livermore National Laboratory's (LLNL) Optical Sciences Laser (OSL) facility [5]. OSL is a large aperture tripled-Nd:Glass laser that has an approximate output energy at 1053 nm (1ω) of 180 J. The 1ω beam is frequency-doubled and tripled using a Type II/Type II conversion scheme with KDP/DKDP crystals. The tripling crystal is detuned ~10 mrad to allow 2ω operation. The 2ω OSL beam has a range of diameters depending on the choice of apertures in the 1ω section of the laser and choice of lenses in the 2ω portion of the laser. The 2ω beam is image-relayed to the sample from the doubling crystal and can have 1/e full-widths of 0.8 – 3.5 cm at the sample depending on the choice of apertures and lenses. The beam spatial profile is nominally a "top-hat" (as seen in Figure 2a.) with a somewhat super-gaussian profile across its top 10%. This variation has proved invaluable in making the scatter as a function of fluence measurements as will be discussed below. The beam typically has a 15% contrast. OSL also has the capability to operate at a variety of pulse widths, namely from ~0.05 – 30 ns. Temporally, the pulse shape is nearly gaussian. Figure 2b.) shows a temporal measurement of a nominal 3 ns pulse. Typically, the OSL pulse durations have a ±10% variation from shot-to-shot. Also, unless otherwise stated, the fluences that will be reported for the OSL shots will be the mean value for the fluence across the "top-hat" portion of the beam, which corresponds to approximately the top 10% of the beam.

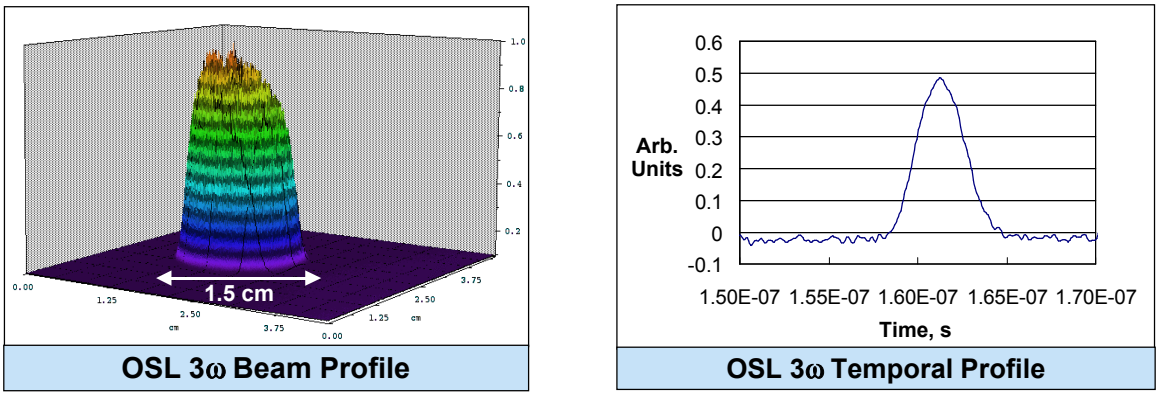

a.) b.)

Figure 2: a.) Spatial profile of the OSL beam at the sample plane for an 8 J/cm^2, 3 ns shot at 3ω. b.) Corresponding temporal profile as measured on a photodiode for the OSL shot in a.).

The 8.3 ns and 23 ns laser raster-conditioning was accomplished in LLNL's Phoenix conditioning facility [5]. A XeF excimer laser that operates at 351 nm, 23 ns with a pulse repetition frequency of 100 Hz is one laser used for the conditioning experiments. This excimer laser has an effective FWHM pulselength of ~23 ns and maximum output energy of ~280 mJ [7]. The depth of focus of the excimer beam at the sample is about 2 mm and the focus is typically positioned at the center of the part (in the direction of propagation). The excimer laser has excellent beam pointing stability and outputs a randomly polarized beam. A pair of polarizers was inserted into the excimer beam path to produce a polarized beam for use in the conditioning scans.

The other laser available in the Phoenix laboratory for conditioning is another XeF excimer laser that operates at 351 nm, 8.3 ns with a pulse repetition frequency of 200 Hz. This excimer laser is aligned to have an effective FWHM pulselength of 8.3 ns and maximum output energy of ~150 mJ. The depth of focus of the excimer beam at the sample is about 10 mm and the focus is typically positioned at the center of the part (in the direction of propagation). The excimer laser has excellent beam pointing stability and outputs a randomly polarized beam. A pair of polarizers was inserted into the excimer beam path to produce a polarized beam for use in the conditioning scans.

2.2 Experimental Plans

Two different types of experiments were performed. The samples used for the experiments were rapid-growth KDP oriented for type I doubling at 1ω. 15 x 15 x 1-cm^3 plates were fabricated out of cut-offs of boules D10 and D11 grown by Cleveland Crystals, Inc. for the National Ignition Facility (NIF). The surfaces of the samples were prepared with a diamond bit-turned finish. Two 15-cm samples were used in this study and will be denoted as D10-1UA and D11-3.

The first set of experiments involved performing single-shot damage tests in OSL at 2ω using pulselengths in the range 0.3 - 10 ns. The 1.2-cm OSL beam was used for these experiments where virgin regions of the samples were exposed to single shots at each site at a variety of fluences for each pulselength. The samples were then photographed using a damage mapping system (DMS) [5,8] set-up which produced a 16-bit digital image of each sample. The digital image will be used to measure scatter as a function of fluence as will be discussed in the next section.

The second set of experiments was performed in two parts. First, virgin regions of crystal D10-1UA were ramp conditioned in OSL using the 3.5-cm beam separately at 2ω and 3ω with pulselengths of 0.3 ns and 3 ns. Rastering was accomplished in OSL by translating the crystal ½ the OSL beam diameter between shots. The nominal conditioning fluence ramps used in OSL for 3ω at 0.3 ns were 1.0, 1.5, 2.0, 2.5, 3.0 J/cm^2, and at 3 ns were 2, 3, 4, 5, 6, 7, 8 J/cm^2. The nominal conditioning fluence ramps used in OSL for 2ω at 0.3 ns were 1.0, 1.5, 2.0, 2.5, 3.0, 3.5, 4.0 J/cm^2, and for 3ns were 3, 4, 5, 6, 7, 8, 9, 10, 11, 12 J/cm^2. Unconditioned or virgin regions of crystal D11-3 were raster-scanned in

Phoenix at 3ω, 8.3 ns and 23 ns. The nominal conditioning fluence ramps used in Phoenix for 3ω for 8.3 ns were 2, 4, 6, 8, 10 J/cm^2 and for 23 ns were 10, 15, 20, 25, 30 J/cm^2. A 90% spatial fluence overlap was used in the raster-conditioning in Phoenix and one scan per fluence was performed. The second part of the experiment tested the conditioned regions of the crystals using the 0.9-cm beam in OSL. The testing consisted of single-shots at 2ω with pulselengths of 0.8, 3, 10 ns at a wide range of fluences. The samples were then photographed using a DMS set-up which produced a 16-bit digital image of each sample. The digital image will be used to measure scatter as a function of fluence as will be discussed in the next section.

2.3 Measuring scatter as a function of fluence

Bulk damage in crystals typically consists of small micro-cavities [6] which will be referred to as "pinpoints". Under illumination of light these pinpoints scatter light like small particles. The scatter signal can be captured in a digital image in terms of bit counts on the pixels of the CCD. The pixels in the damage image can then be related to the corresponding damaging fluence through the pixels in the fluence image of the damaging beam yielding scatter as a function of fluence. Figure 3 illustrates the process in which bulk damage scatter as a function of damaging fluence is extracted from an image of the damage in the crystal and the corresponding image of the damaging beam's fluence spatial profile. The first step in the process is to damage a region on a crystal and record an image of the damaging beam's spatial fluence profile. The next step (step 2 in Figure 3) is to obtain a damage or scatter map of the damaged region in the crystal. The damage map needs to be a linear image of the luminosities as recorded by the CCD. The damaging beam's spatial profile is then registered to the damage map collected from the crystal. The two images are scaled and rotated until features in the beam's spatial profile overlay with corresponding features in the damage image. The registered images are then divided into 5 pixel x 5 pixel subsets where the average fluence and scatter luminosity is respectively calculated in each 5 x 5 subset throughout each image. We have determined that performing the average over 5 x 5 pixel subsets optimizes noise reduction without losing resolution. The third step is to plot corresponding registered pairs of scatter (averaged over 25 square pixels) vs. fluence (averaged over 25 square pixels) to obtain the scatter as a function of fluence curve as shown in step 3 of Figure 3. The noise in the scatter data is believed to be due to registration errors between the two images, focus error in the damage image, and possibly moderate scale non-uniformities in the crystal. It was determined that plotting the data as ordered (rather than x-y registered) pairs produces a smooth well-behaved curve through the center of the noise in the x-y registered data. In other words, the ordered plot of the data as shown in step 4 Figure 3 is very close to a best fit to the data in step 3 Figure 4. The ordering is carried out by first sorting the fluence data from lowest to highest value independent of the scatter data and then sorting the scatter data similarly. Then the two sets of data are put into one to one correspondence and plotted as shown in step 4 Figure 3. For the current work, this technique may be considered the equivalent of ensemble smoothing the data (which yields similar results). A study demonstrating the feasibility and utility of this technique is currently being examined. The ordered pairs plot is a sensible way to present the data if the bulk damage is an increasing function of the fluence, the majority of the error sources are random, and if the registration errors are not too large. The contribution to the noise in the registered pairs plots has been investigated by the authors and it has been concluded that it is very reasonable to use the ordered data for analysis. Therefore the following analysis in this report will solely use the ordered pair data.

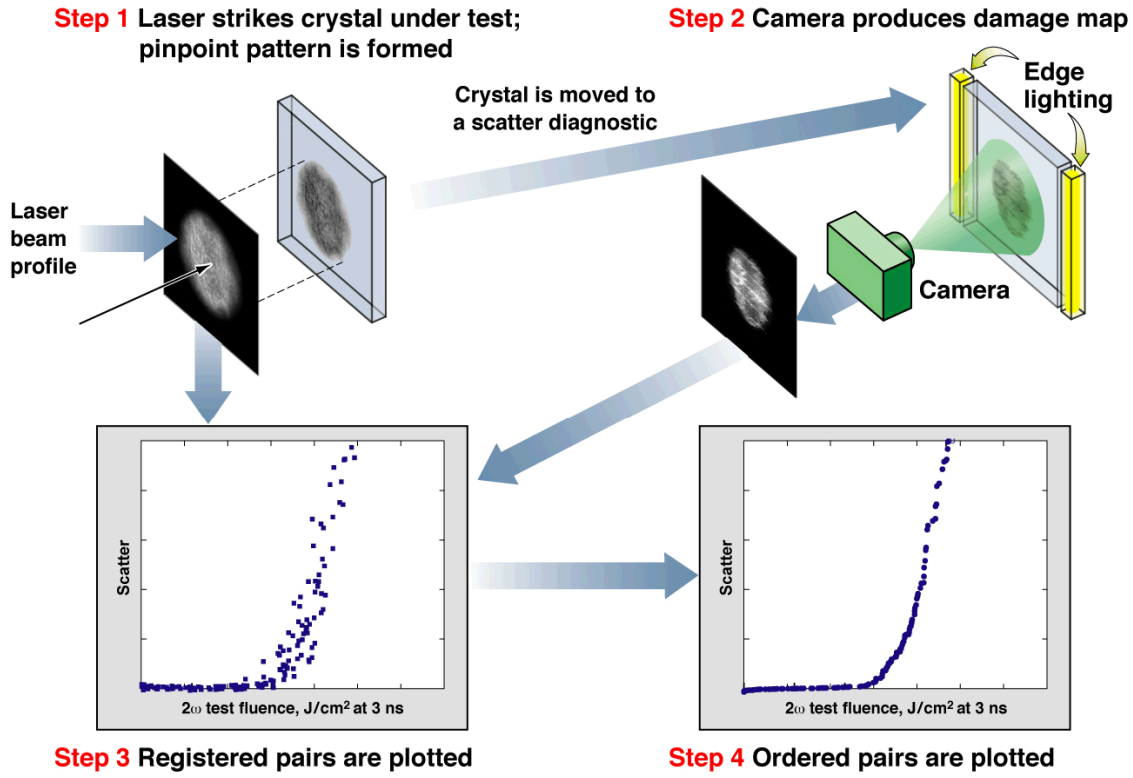

Figure 3: Process steps to extract bulk damage scatter as a function of damaging fluence data. The data is extracted from an image of the damaged region in the crystal and the corresponding image of the damaging beam's fluence spatial profile. The damage map of the damage in the crystal is a 16-bit digital image file.

3. RESULTS AND ANALYSIS

3.1 Damage map of D10-1UA

Figure 4 shows a damage map of crystal D10-1UA after single-shot damage testing at 2ω on both unconditioned and conditioned material. The single-shot damage testing was conducted with several OSL beam diameters. (i.e. 0.9, 1.2, and 1.5-cm). The ramp conditioning in OSL at 2ω and 3ω was performed using the 3.5-cm beam where at 2ω 0.3 ns the 2.5-cm beam was used. The white boxes in Figure 4 denote the approximate region ramp-conditioned with the protocol as labeled. The white labels within the image show the 2ω single-shot damage test shots' fluence and pulselength. The shots labeled outside the white boxes are single-shot damage tests on unconditioned regions of the crystal. Note the paucity of damage in the 3ω, 0.3 ns conditioned region. An outline of the 3.5-cm conditioning beam can be seen in the 2ω, 0.3 ns conditioned region, which is due to laser cleaning of the surface of the crystal as the ramp-conditioning was performed.

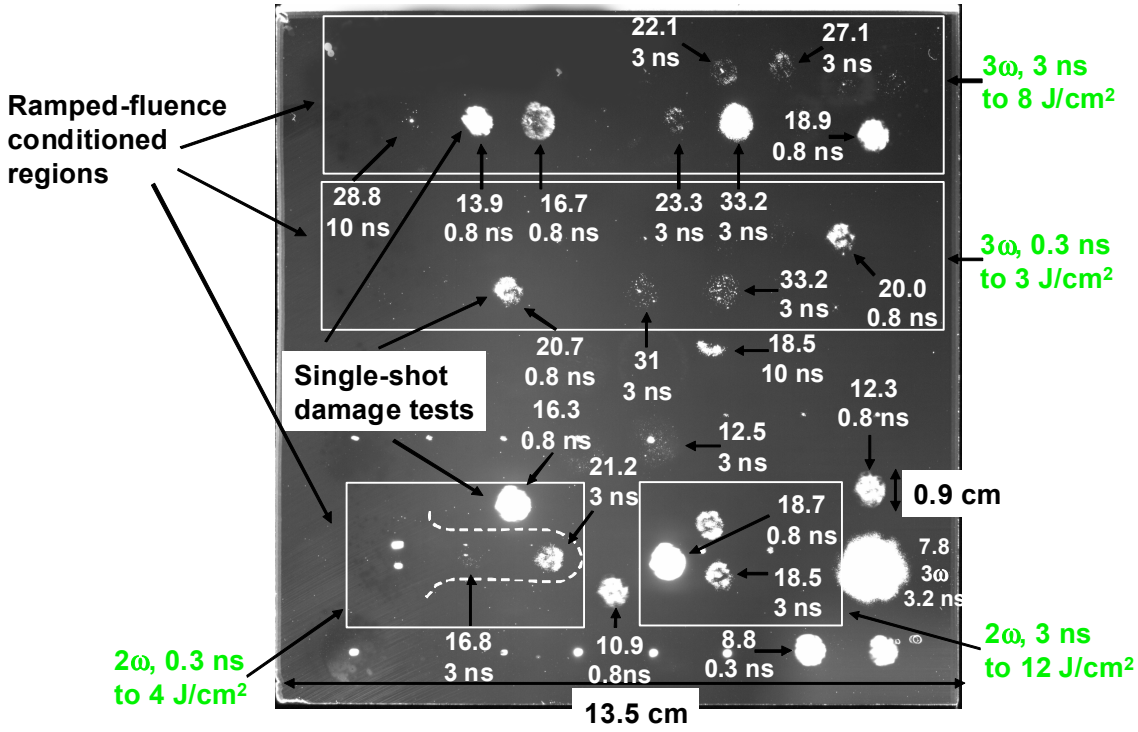

Figure 4: Damage map of KDP crystal D10-1UA after conditioning and damage testing in OSL. The white boxes denote the approximate region ramp-conditioned as labeled with the conditioning protocol's wavelength, pulselength, and peak conditioning fluence. The white numeric labels show the 2ω single-shot damage test shots' fluence and pulselength. Note, not all shots visible in the figure are labeled. A single site on an unconditioned region was single-shot tested at 3ω, 3ns as labeled.

The faint diagonal lines near the lower left corner of D10-1UA that look like tiny parallel scratches are grooves seen from the diamond finishing tool. The ~ 2mm "hot-spot" seen within many of the shots and in cases by itself is believed to be a ghost reflection from within the OSL beamline at a substantially higher intensity. This "hot-spot" is estimated to have between a 20-30% higher intensity than the average top 10% of the rest of the beam. The double-imaged scattering site near the upper-left hand edge of the 3ω, 3ns conditioned region is a fiducial applied to the part with water for use as a positioning aid during the OSL shots. The two sets of double images seen near the lower right-hand corner of the part are also fiducials. The "arc-like" appearance of the 18.5 J/cm^2, 10 ns test shot near the lower edge of the 3ω, 0.3 ns conditioned region is due to the influence of the 3ω, 0.3 ns conditioned region encroaching partially across the test shot aperture. Upon inspection by "eye", it can be seen that the 3ω, 0.3 ns conditioned region performed best at all pulselengths. Crystal D11-3 was conditioned in the Phoenix laboratory as described above and then 2ω tested and analyzed in a similar manner to D10-1UA.

3.2 Unconditioned results

3.2.1 Scatter vs. fluence

Analysis of the test shots on the unconditioned region of D10-1UA to determine scatter as a function of fluence was performed as described in section 2.3. Figure 5 shows the results for scatter vs. 2ω damaging fluence for the single-shot damage testing of unconditioned regions on D10-1UA at 4 different pulselengths. Figure 5 reveals that there is less scatter at a fixed fluence for longer pulselengths. The size of the pinpoints has been observed to be an approximately linear function of the damaging pulselength [6, 9], therefore the higher amounts of scatter in Figure 5 correspond to higher damage density. The damaging fluence for equivalent scatter at 10 ns is ~4X greater than the fluence at 0.3 ns as generally expected for dielectrics [6, 10]. The results also show that for all of the damaging pulselengths the damage density or scatter is a strong function of the damaging fluence ($\phi^{\sim 5}$).

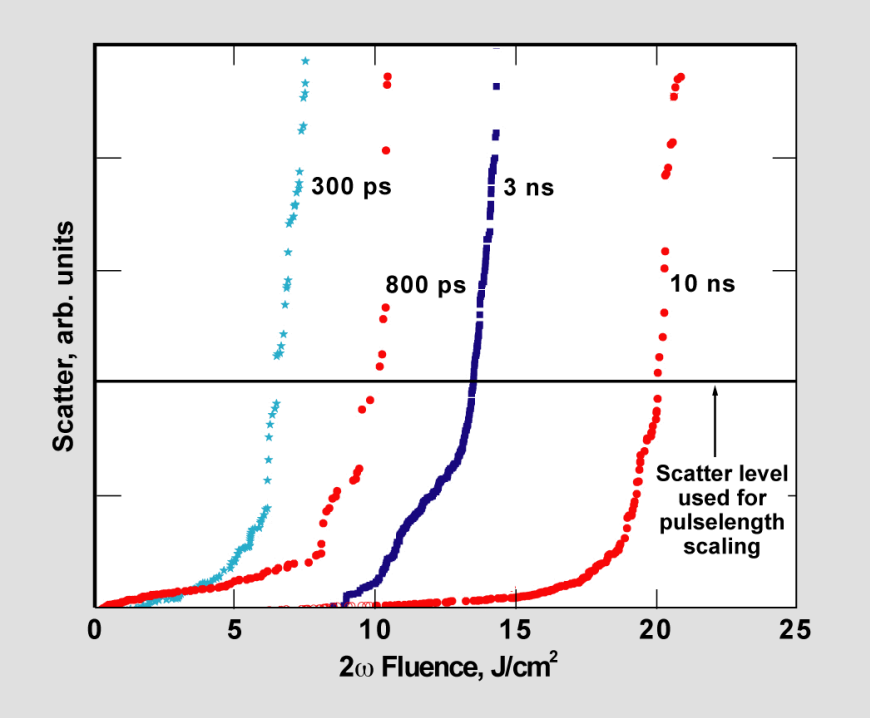

Figure 5: Plot of ordered pairs of scatter vs. damaging fluence extracted from the damaging beam and damage map images as described in section 2.3, for unconditioned KDP at the pulselengths labeled for the 2ω damaging pulses. Analysis of the 18.5 J/cm^2 10 ns, 12.5 J/cm^2 3 ns, 10.9 J/cm^2 0.8 ns, 7.8 J/cm^2 0.3 ns shots is presented. The 7.8 J/cm^2 0.3 ns shot is not labeled in Figure 4. The reference level for scatter used for the pulselength-scaling derivation in section 3.4 is denoted.

3.3 Conditioned results

3.3.1 Scatter vs. fluence for testing at 2ω, 3ns

Analysis of the 2ω, 3 ns test shots on the conditioned regions of D10-1UA and D11-3 to determine scatter as a function of fluence was performed as described in section 2.3. Figure 6 shows the results for scatter vs. 2ω, 3 ns test fluence for testing of the conditioned regions on D10-1UA and D11-3. Also shown in Figure 6 for comparison are the results for unconditioned D10_1UA tested at 2ω, 3 ns. The labels for the various curves specify the *conditioning* wavelength and pulselength for the region tested as well as the measured peak fluence obtained during the conditioning ramp. The 3ω,

8.3 ns and 23 ns data is labeled "(estimate)" because the unconditioned performance of D10-1UA and D11-3 were different. The 8.3 ns and 23 ns data were adjusted by shifting each by the difference in the unconditioned performance between D10-1UA and D11-3 (shift of -1.5 J/cm^2 calculated at equivalent scatter levels). Also, for 3ω conditioning at pulselengths of 3, 8.3, and 23 ns, surface damage limited the peak conditioning fluence to the values shown. The results in Figure 6 show that for all of the conditioning protocols the scatter vs. test fluence is again a strong function of the damaging fluence ($\phi^{\sim 5}$) for all conditioning pulselengths.

For the 2ω, 0.3 ns and 3 ns conditioning protocols, the peak fluence obtained in the conditioning ramp was limited by the 2ω output of OSL. Recent work [11] suggests 2ω, 3 ns to have a greater conditioning effect than that shown by the 2ω, 3 ns conditioning in this work. This difference is possibly due to the relatively low peak conditioning fluence used here which did not fully access the conditioning effect, use of different numbers of conditioning pulses at each fluence step in the ramp, or may be due to differences in experimental set-up. As can be seen in Figure 6, the 3ω, 0.3 ns conditioned material had the best performance among the protocols tested with an approximate 3X increase in performance over unconditioned. The 3ω, 3 ns conditioning had the next best performance with an approximate 2X increase in performance over unconditioned. We only see an ~10% increase in the performance following excimer conditioning at either 8.3 ns or 23 ns.

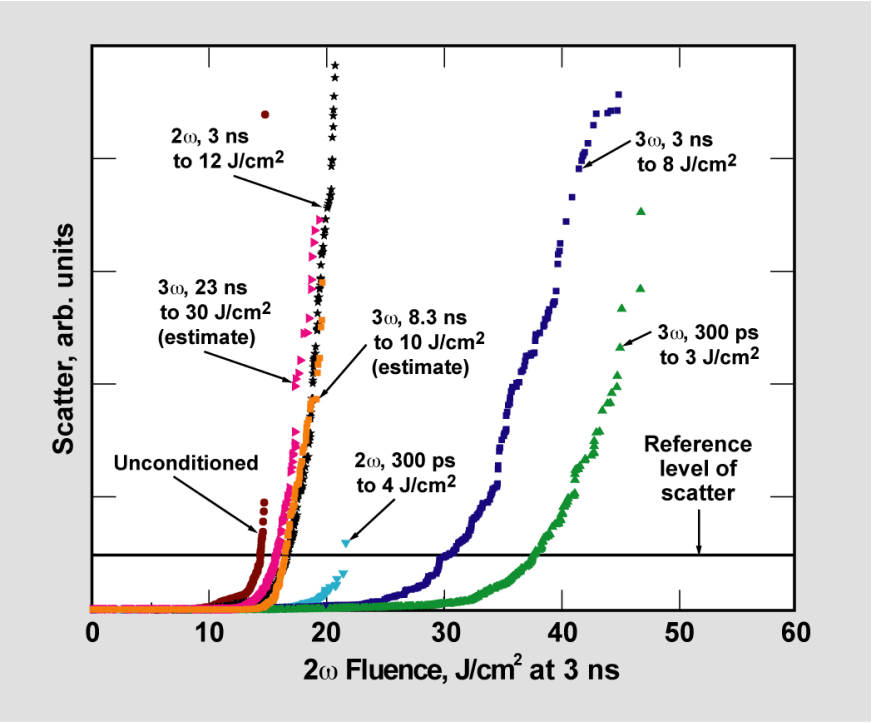

Figure 6: Plot of ordered pairs of scatter vs. damaging fluence extracted from the damaging beam and damage map images as described in section 2.3, for 2ω, 3 ns testing on the conditioned regions of D10-1UA (Figure 4) and D11-3. The labels give the wavelength and pulselength used for the *conditioning* and the peak fluence achieved during the conditioning ramp. The unconditioned data is shown for comparison. The 3ω, 8.3 ns and 23 ns data is shown labeled "(estimate)" because the unconditioned performance of D10-1UA and D11-3 were different. The reference level of scatter used in the discussion of differences in the performance among the various wavelength and pulselength-conditioned regions is labeled on the figure.

3.3.2 Comparison of conditioning wavelengths and pulselengths

To alternatively illustrate the relative performance of the conditioning protocols when tested at 2ω, 3 ns, Figure 7 shows a plot of test fluences corresponding to the reference level of scatter from Figure 6. The level for unconditioned damage performance is also labeled in Figure 7 and has an experimental uncertainty of ± 1 J/cm^2. The increase in conditioning effectiveness with decreasing pulselength seen in Figure 7 implies that the level of conditioning obtained at a given pulselength is a function of both the fluence and irradiance applied to the material as shown in previous work using 3ω light [12]. Figure 7 shows that there appears to be a general trend that shorter wavelengths and shorter pulselengths provide better conditioning. Based on our previous work with 3ω [12], we would expect the curves in Figure 7 to roll over towards unconditioned performance for conditioning pulselengths less than ~ 300 ps. In the range of 3ω conditioning pulselengths between 0.3 ns and 3 ns, we find the sensitivity in the improvement in fluence of the scatter curves after conditioning to variation in conditioning pulselength to be ~1 J/cm^2/ns. This sensitivity is about twice what was found for 3ω conditioning under 3ω, 3 ns testing [12]. For 3ω conditioning pulselengths >3 ns, surface damage limits the peak (maximum) conditioning fluence which implies that the fall-off in the performance of the >3ns conditioned material seen here is reasonable and important from a practical point of view.

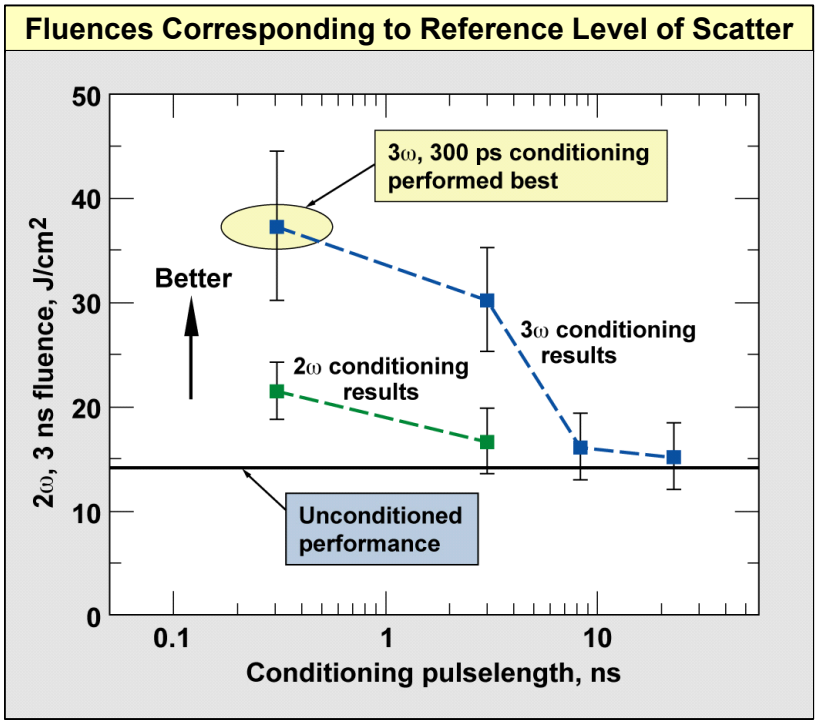

Figure 7: Plot of 2ω, 3 ns test fluences corresponding to the reference level of scatter from the various conditioning wavelength and pulselength combinations as described in Figure 6. The 3ω, 300 ps conditioning protocol performed best. The error bars are the widths of the scatter vs. fluence plots (not shown) before any ordering measured at the reference level of scatter.

3.3.3 Scatter vs. fluence for testing of 3ω, 3 ns conditioning

Analysis of the test shots on the 3ω, 3ns conditioned region of D10-1UA to determine scatter as a function of fluence was performed as described in section 2.3. Figure 8 shows the results for scatter vs. 2ω damaging fluence for damage testing of the 3ω, 3 ns conditioned region on D10-1UA at 3 different pulselengths. Figure 8 reveals that there is less

scatter at a fixed fluence for longer damaging pulselengths for conditioned KDP. The damaging fluence for equivalent scatter at 10 ns is ~2X greater than the fluence at 0.8 ns as generally expected for dielectrics [6, 10]. The results also show that at all of the damaging pulselengths the damage density or scatter is a strong function of the damaging fluence ($\phi^{\sim 5}$).

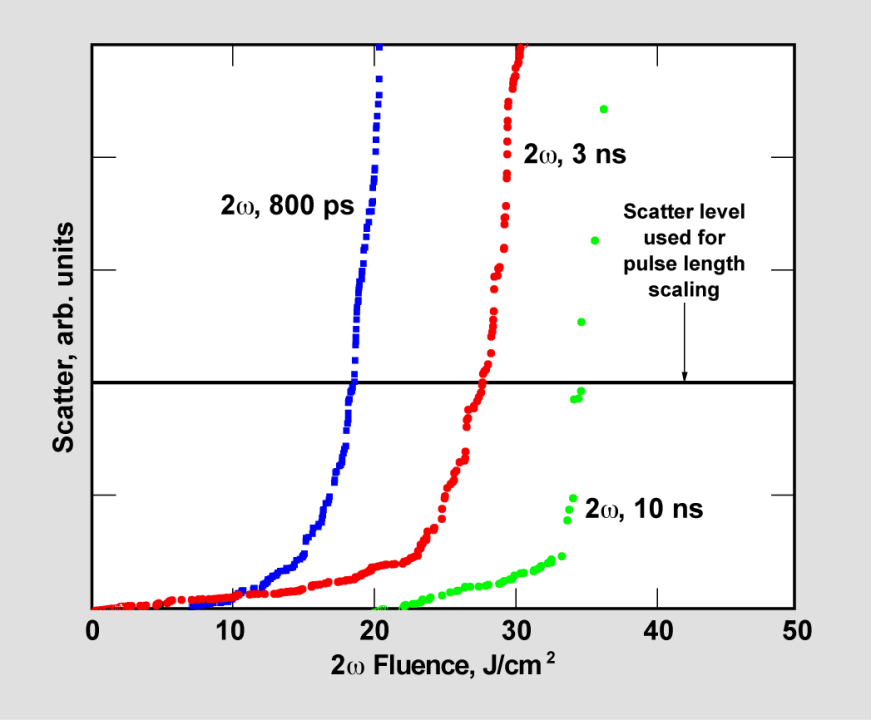

Figure 8: Plot of ordered pairs of scatter vs. 2ω damaging fluence extracted from the damaging beam and damage map images as described in section 2.3, for 3ω, 3ns conditioned KDP at the pulselengths labeled for the 2ω damaging pulses. Analysis of the 28.8 J/cm^2 10 ns, 33.2 J/cm^2 3 ns, 18.9 J/cm^2 0.8 ns shots is presented. The reference level for scatter used for the pulselength-scaling derivation is denoted.

3.4 Pulselength-scaling

The fluences corresponding to the reference levels of scatter as shown in Figures 5 and 8 are used to derive the pulselength-scaling relationships for both the unconditioned and conditioned KDP. The reference level of scatter is chosen out of convenience. Other levels of scatter were used for the pulselength-scaling derivation and the results for the exponents in general agreed with that shown in Figure 9 to within approximately ±0.05. Figure 9 shows a plot of the 2ω fluences corresponding to the reference levels of scatter from Figures 5 and 8. The line through each data set is a numerical fit of $a\tau^b$ where a and b are fitting parameters. The results of the fits are 2ω fluence pulselength-scaling relationships for equivalent scatter of $\tau^{0.30 \pm 0.11}$ for unconditioned KDP and of $\tau^{0.27 \pm 0.14}$ for 3ω, 3 ns conditioned KDP. The uncertainty to the exponents is the determined by fits to the extrema of the data. This is the first systematic determination of 2ω damaging fluence pulselength-scaling for same scatter in either unconditioned or conditioned KDP. Essentially what we find is that unconditioned KDP and 3ω, 3ns conditioned KDP have the same 2ω damaging fluence pulselength-scaling based on scatter. A pulselength-scaling relationship for scatter of $\tau^{\sim 0.3}$ is plausible if the thermal model of Feit and Rubenchik is valid [13, 14], if the distribution of precursors is a power function [13, 14], and if the damage site size (pinpoint size) for Gaussian pulses varies linearly with pulselength [9]. Interestingly, these pulselength-scaling results for same scatter are equivalent to results from the current authors [12] and by Runkel et al. [6] for *3ω* damaging fluences for equivalent pinpoint density. Understanding the physical reason for this agreement is currently being pursued by the authors.

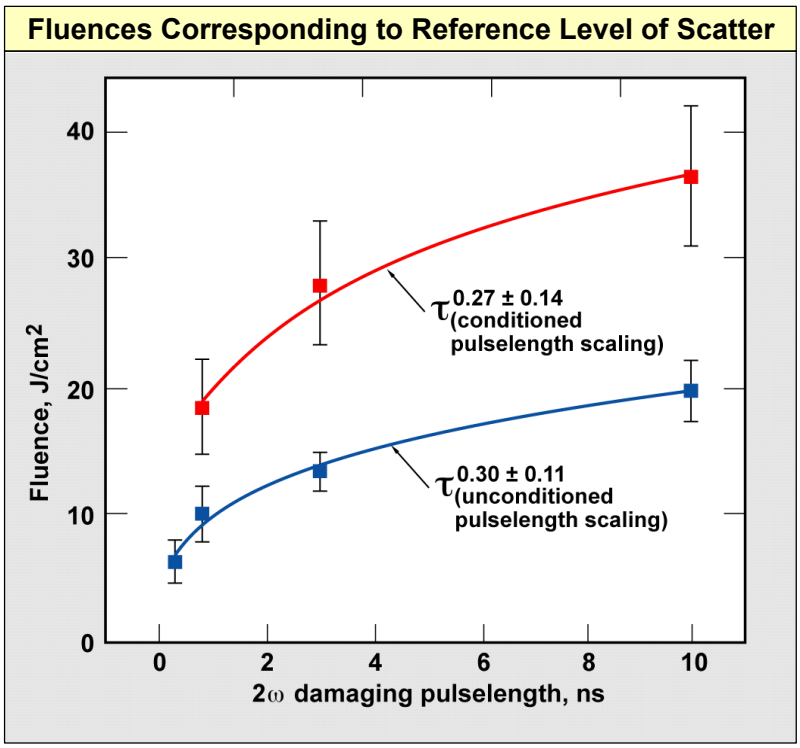

Figure 9: Plot of 2ω fluences (at the reference level of scatter) vs. 2ω test pulselength from Figures 5 and 8. The lines are numerical fits of $a\tau^b$ to each data set. The error bars are the widths of the scatter vs. fluence plots (not shown) before any ordering measured at the reference level of scatter. The result of the fits are 2ω fluence pulselength-scaling relationships for equivalent scatter of $\tau^{0.30 \pm 0.11}$ for unconditioned KDP and of $\tau^{0.27 \pm 0.14}$ for 3ω, 3 ns conditioned KDP. The error to the exponents is the difference between the fits shown and fits to the extrema of the error bars on the 0.3, 0.8 and 10 ns data points in both graphs.

4. SUMMARY

Bulk damage in unconditioned material was studied in terms of scatter vs. 2ω damaging fluence at pulselengths of 0.3, 0.8, 3, and 10 ns. It was found that there is less scatter at fixed fluence for longer pulselengths. The size of the pinpoints has been shown elsewhere to be an approximately linear function of the damaging pulselength [6, 9], therefore higher amounts of scatter correspond to a higher damage density. The results also show that at all pulselengths the scatter is a strong function of the 2ω damaging fluence ($\phi^{\sim 5}$). From the unconditioned data, it is determined that 2ω damaging fluences for equivalent scatter scale as $\tau^{0.30 \pm 0.11}$ over ~two orders of magnitude of pulselength. For 3ω, 3 ns conditioned KDP we find a fluence pulselength-scaling for equivalent scatter of $\tau^{0.27 \pm 0.14}$. We note that the 2ω fluence pulselength-scaling (based on scatter) for unconditioned and conditioned KDP agree. These pulselength-scaling results are consistent with past work by other authors [6, 12]. Scatter as a function of fluence was also measured for conditioned KDP tested at 2ω at pulselengths of 0.8, 3, 10 ns to evaluate the degree of conditioning. The conditioning protocols tested were fluence ramps at either 3ω with pulselengths of 0.3 ns, 3ns, 8.3 ns, and 23 ns, or at 2ω at 0.3 ns and 3ns. For conditioned KDP, the results show that at all test pulselengths the scatter is again a strong function of the 2ω damaging fluence ($\phi^{\sim 5}$). For the conditioning protocols tested, doubler-cut KDP conditioned at 3ω with 300 ps pulses had the highest 2ω damage resistance. A general trend is revealed where shorter wavelengths and shorter pulselengths are apparently better at conditioning for 2ω, 3ns damage. The sensitivity (derivative) of the conditioning effectiveness to the conditioning

pulselength at 3ω between 0.3 ns and 3 ns is found to be ~ 1 J/cm^2/ns. Surface damage was found to limit the peak conditioning fluences for conditioning pulselengths >3 ns.

ACKNOWLEDGEMENTS

The authors wish to thank Mark McDaniel for the artwork and Eric Miller and Heather Platz for cleaning and coating the crystals used in this work, all with LLNL. This work was performed under the auspices of the U.S. Department of Energy by the University of California, Lawrence Livermore National Laboratory under contract No. W-7405-Eng-48.

REFERENCES

1. J. J. De Yoreo, A. K. Burnham, P. K. Whitman, "Developing KH_2PO_4 and KD_2PO_4 crystals for the world's most powerful laser," Int. Mater. Rev. **47**, 113 (2002)
2. N. P. Zaitseva, J. Atherton, R. Rozca, L. Carmen, I. Smolsky, M. Runkel, R. Lyon, and L. James, J. of Crystal Growth **197**, 911 (1999)
3. M. Runkel, S. Maricle, R. Torres, J. Auerbach, R. Floyd, R. Hawley-Fedder, and A. Burnham, "Effect of thermal annealing and second harmonic generation on bulk damage performance of rapid growth KDP type I doublers at 1064 nm", 2000 SPIE Proceedings, **4347**, 389 (2001)
4. M. Runkel, K. Neeb, M. Staggs, J. Auerbach, A. K. Burnham, "The results of raster-scan laser conditioning studies on DKDP triplers using Nd:YAG and excimer lasers," 2001 SPIE Proceedings, **4679**, 368 (2002)
5. M. Runkel, J. Bruere, W. Sell, T. Weiland, D. Milam, D. Hahn, M. Nostrand, "Effects of pulse duration on bulk laser damage in 350-nm raster scanned DKDP," 2002 SPIE Proceedings, **4932**, 405 (2003)
6. M. Runkel, A. K. Burnham, D. Milam, W. Sell, M. Feit, A. Rubenchik, "The results of pulse-scaling experiments on rapid-growth DKDP triplers using the Optical Sciences Laser at 351 nm," 2000 SPIE Proceedings, **4347**, 359 (2001)
7. M. Runkel, "Some commonly used calculations in small beam damage testing: Effective area, effective pulse durations, and pulse scaling," NIF report # (October 1, 2002)
8. F. Rainer, "Mapping and inspection of damage and artifacts in large-scale optics," 1996 SPIE Proceedings, **3244**, 272 (1997)
9. C. W. Carr, M. D. Feit, A. M. Rubenchik, J. B. Trenholme, "Summary of recent experiments in bulk damage initiation and their interpretation," 2005 SPIE Boulder Damage Symposium, paper 5991-28
10. B. C. Stuart, M. D. Feit, S. Herman, A. M. Rubenchik, B. W. Shore, and M. D. Perry, "Nanosecond-to-femtosecond laser-induced breakdown in dielectrics," Phys. Rev. B, **53**, 1749 (1996)
11. P. DeMange, C. W. Carr, R. A. Negres, H. B. Radousky, and S. G. Demos, "Multiwavelength investigation of laser-damage performance in potassium dihydrogen phosphate after laser annealing," Opt. Lett., **30**, 221 (2005)
12. J. J. Adams, T. L. Weiland, J. R. Stanley, W. D. Sell, R. L. Luthi, J. L. Vickers, C. W. Carr, M. D. Feit, A. M. Rubenchik, M. L. Spaeth, R. P. Hackel, "Pulse length dependence of laser conditioning and bulk damage in KD_2PO_4," 2004 SPIE Proceedings, **5647**, 265 (2004)
13. M. D. Feit and A. M. Rubenchik, "Implications of nanoabsorber initiators for damage probability curves, pulse length scaling, and laser conditioning," 2003 SPIE Proceedings, **5273**, 74 (2004)
14. M. D. Feit, A. M. Rubenchik, J. B. Trenholme, "Simple model of laser damage initiation and conditioning in frequency conversion crystals," 2005 SPIE Boulder Damage Symposium, paper 5991-17